Improved forgetting factor recursive least square and adaptive square root unscented Kalman filtering methods for online model parameter identification and joint estimation of state of charge and state of energy of lithium-ion batteries.

ZHU, T., WANG, S., FAN, Y., ZHOU, H., ZHOU, Y. and FERNANDEZ, C.

2023

Improved forgetting factor recursive least square and adaptive square root unscented Kalman filtering methods for online model parameter identification and joint estimation of state of charge and state of energy of lithium-ion batteries

Tao Zhu[1] · Shunli Wang[1,2] · Yongcun Fan[1] · Heng Zhou[1] · Yifei Zhou[1] · Carlos Fernandez[3]

[1] School of Information Engineering, Southwest University of Science and Technology, Mianyang 621010, China

[2] School of Electrical Engineering, Sichuan University, Chengdu 610065, China

[3] School of Pharmacy and Life Sciences, Robert Gordon University, Aberdeen, UK

Abstract

The estimation of the state of charge (SOC) and state of energy (SOE) of lithium-ion batteries is very important for the battery management system (BMS) and the analysis of the causes of equipment failures. Aiming at many problems such as the changes in the parameters of the lithium battery model and the accurate estimation of the SOC and SOE, this paper proposes a joint algorithm of forgetting factor recursive least square (FFRLS) and adaptive square root unscented Kalman filter (ASRUKF) based on the second-order RC equivalent circuit model. In this paper, the joint FFRLS-ASRUKF algorithm is used to perform simulation experiments under three different working conditions of HPPC, DST, and BBDST at different temperatures of 25, 15, and 5 °C. And a current ± 1 A offset is added as a disturbance to verify the robustness of ASRUKF. The results show that under HPPC working condition, the RMSE, MAE, and MAPE estimated by ASRUKF for SOC and SOE of lithium-ion batteries at three temperatures do not exceed 0.0016, 0.0012, and 0.43%, respectively. Under DST working condition, ASRUKF estimates that RMSE, MAE, and MAPE of SOC and SOE of lithium-ion batteries at three different temperatures do not exceed 0.0013, 0.0009, and 0.70% respectively. Under BBDST operating conditions, ASRUKF estimates that the RMSE, MAE, and MAPE of the SOC and SOE of lithium-ion batteries at three different temperatures do not exceed 0.0016, 0.0009, and 0.71% respectively. After adding the current offset, ASRUKF can still accurately estimate the SOC and SOE of lithium-ion batteries.

Keywords Lithium-ion battery ; Second-order RC equivalent circuit model ; State of charge ; State of energy ; Adaptive square root unscented Kalman filter algorithm ; Forgetting factor recursive least squares

Introduction

The transportation sector and other industries view electric vehicles (EVs) as the primary form of transportation for future global warming due to the increased mining and consumption of fossil fuels including coal, oil, and natural gas as well as the growing demand to combat global warming [1]. At the same time, clean energies such as wind and solar power are being researched and developed in departments around the world [2]. Lithium-ion batteries are widely used in electric vehicles, solar power generation, wind power generation, and other fields because of their no memory, large energy storage capacity, less self-discharge, high energy density, long cycle life, and low maintenance costs [3–5].

The battery's remaining capacity is referred to as the battery's state of charge (SOC). Its value is the proportion of the battery's rated capacity to its remaining capacity under specific discharge conditions [6]. SOE is the ratio of the energy that can be released by the battery under current conditions to the maximum available energy of the battery. By fully utilizing the SOC and SOE, the remaining energy and state of the battery can be determined [7–9]. Accurately estimating the SOC and SOE of a battery pack is therefore a key factor in effective battery management, safe driving, and normal use of instruments and equipment [10]. Due to aging and obvious nonlinear behavior, battery characteristics have changed considerably during its life [11]. Estimating SOC and SOE is therefore a challenging task.

There are many SOC estimation methods, including the ampere–hour integration method, open circuit voltage method, discharge experiment method, load voltage method, internal resistance method, neural network algorithm, Kalman filter algorithm, and fuzzy logic algorithm [12–14]. Among them, Kalman filtering algorithms are more commonly used, such as extended Kalman filter algorithm (EKF) and unscented Kalman filter algorithm (UKF) [15]. EKF algorithm is a process of linearizing nonlinear systems through partial derivative and first-order Taylor expansion, which may lead to performance degradation. UKF algorithm solves the problem of filtering through traceless transformation [16–19]. It is a numerical sampling technique that

deterministically finds the smallest sigma point set to estimate the mean and variance of state variables under nonlinear transformation. In engineering applications, the UKF algorithm is susceptible to anomalous disturbances, initial value errors, and Cholesky's effect on non-semi-positive definite matrices, which leads to divergence of the system [20]. UKF and EKF have similar robustness, but the problem of parameter selection has not been completely solved, and the filtering effect is also affected by the initial value of filtering as well as the EKF algorithm [21–23]. Unlike the traditional unscented Kalman filter, the square root of the state covariance matrix is propagated directly in the square root unscented Kalman filter algorithm (SRUKF), avoiding the calculation of the square root of the state covariance in each iteration step [24–27]. SRUKF has better numerical properties, which not only solves the short-comings of EKF and UKF but also ensures the positive semi-determinism of the state covariance matrix [28–30]. All three filtering methods mentioned above can achieve good performance under certain assumptions. However, these assumptions are usually not fully satisfied.

In addition, the accuracy of estimation greatly depends on how well the equivalent model characterizes the dynamic properties of the cell [31–33]. The common types of battery modeling available today are electrochemical models, machine learning models, equivalent circuit models, and neural network models [34]. The complexity of electro-chemical models is high, and practical applications may not meet the theoretical requirements [35]. Neural network models require more data compared to traditional models. The equivalent circuit model uses circuit elements such as resistors and capacitors to form a circuit network to simulate the dynamic voltage response characteristics of the battery. The commonly used equivalent circuit models include the Rint model, Thevenin model, PNGV model, and second- order RC equivalent model [36–38].

And how to accurately identify the parameters in the lithium-ion battery model is also the focus of the whole SOC estimation process. Recursive least square (RLS) identifies the parameters of the system model by minimizing the sum of squares of the generalized errors based on least square (LS) [39]. However, as the number of iterations of the algorithm data increases, the values of the gains K and P become smaller and smaller, which makes the error of parameter identification larger and larger. The forgetting factor can be added to the RLS discrimination to improve the online estimation capability of the RLS algorithm [40]. The effect of the forgetting factor is to give less weight to the older data with longer running time and more weight to the latest observed data during the discrimination process [41].

To overcome these drawbacks, a joint algorithm of forgetting factor recursive least squares and adaptive square root unscented Kalman filter is proposed in this paper for the estimation of SOC and SOE. Among them, FFRLS introduces a genetic factor to make the identification of internal parameters of lithium batteries more accurate. Adaptive square root unscented Kalman filter algorithm is improved based on unscented Kalman filter algorithm to solve the low stability problem of unscented Kalman filter and extended Kalman filter algorithms and to improve accuracy and convergence time.

Mathematical analysis

Definition of SOC and SOE of lithium-ion battery

The SOC of a lithium-ion battery refers to the state of charge, also known as residual charge, which is the ratio of the remaining capacity of the battery after a period of use or long-term storage to its fully charged capacity. The state of energy (SOE) of a lithium battery is the ratio of the energy that can be released under current conditions to the maximum available energy of the battery. It is an important indicator that reflects the energy consumption of the battery. The method of estimating battery SOE is different from SOC, which is affected not only by the battery load current but also by the battery terminal voltage. The formula for calculating the SOC and SOE of lithium-ion batteries using the time integration method is as follows:

$$\begin{cases} \mathrm{SOC} = \mathrm{SOC}_0 - \int_0^t i(t)dt/Q_0 \\ \mathrm{SOE} = \mathrm{SOE}_0 - \int_0^t i(t) \times u(t)dt/Q_0 \end{cases} \tag{1}$$

where SOC and SOC_0 refer to the SOC at the current moment and the previous moment, respectively, $i(t)$ and $u(t)$ refer to the current and voltage, and Q_0 refers to the nameplate capacity.

Second-order RC equivalent circuit model

Considering that the equivalent circuit model can effectively reflect the internal mechanism of the battery, the calculation is simple, and the accuracy of the equivalent circuit model above the second order is not significantly improved, but the calculation amount is greatly increased; the second-order RC model in the equivalent circuit model is finally selected to estimate SOC and SOE.

The second-order RC model is composed of the Thevenin model and an RC circuit. Two resistance capacitance parallel circuits are used to simulate concentration polarization and electrochemical polarization, respectively. Its basic idea is to use two RC networks to describe the polarization effect of the battery in use, which to some extent makes up for the shortcomings that the internal resistance model cannot characterize the dynamic characteristics of lithium-ion batteries and the Thevenin model has a large error. The second-order RC model is shown in Fig. 1.

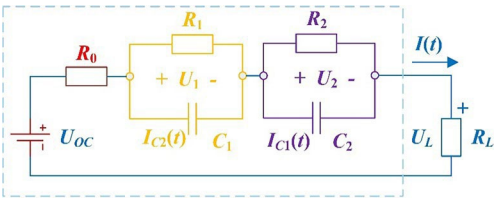

Fig. 1 Second-order RC equivalent circuit model

U_{OC} represents open circuit voltage, U_L represents terminal voltage, R_0 represents ohmic internal resistance, R_1 represents electrochemical polarization internal resistance, C_1 represents electrochemical polarization capacitance, R_2 is the internal resistance of concentration electrode, and C_2 is the capacitance of concentration electrode. The RC circuit composed of R_1 and C_1 represents the stage when the voltage changes rapidly during the chemical reaction inside the battery. The RC circuit composed of R_2 and C_2 represents the stage where the voltage changes slowly during the chemical reaction inside the battery.

Forgetting factor recursive least square method

To increase the feedback effect of new data, the forgetting fac- tor λ ($0 < \lambda < 1$) is introduced and added as a coefficient to the observed data matrix and the system output vector. The closer the value of λ is to 1, the better the simulation. The smaller the value of λ, the better the tracking, as old records disappear quickly. However, fast tracking can lead to unstable estimation results. The FFRLS algorithm is combined with the second-order battery model. The FFRLS algorithm is combined with the second-order battery model to update each parameter of the battery in a timely and accurate manner.

Among them,

$$\begin{cases} k_1 = \frac{-bT-2a}{T^2+bT+a} \\ k_2 = \frac{a}{T^2+bT+a} \\ k_3 = \frac{cT^2+dT+R_0}{T^2+bT+a} \\ k_4 = \frac{-dT-2aR_0}{T^2+bT+a} \\ k_4 = \frac{aR_0}{T^2+bT+a} \end{cases} \tag{2}$$

The least squares mathematical form of discretization can be substituted into the recursive least squares method, using $\theta = [k_1\ k_2\ k_3\ k_4\ k_5]^T$ as a direct identification parameter, and then deriving the circuit model parameters R_0, R_1, R_2, C_1, C_2, from the identification results of these parameters, as follows. Let $k_0 = T^2 + bT + a$, then the value of each parameter can be obtained from Eq. 2 as shown in Eq. 3.

$$\begin{cases} k_0 = T^2/k_1 + k_2 + 1 \\ a = k_0 k_2 \\ b = -k_0\left(k_1 + 2k_2\right)/T \\ c = k_0\left(k_3 + k_4 + k_5\right)/T \\ d = -k_0\left(k_4 + 2k_5\right)/T \\ R_0 = k_5/k_2 \end{cases} \tag{3}$$

Then, let $a=\tau_1\tau_2$ and $b=\tau_1+\tau_2$, then from $\tau^2-b\tau+a=0$, solve for τ_1 and τ_2 as shown in Eq. 4.

$$\begin{cases} \tau_1 = \sqrt{b^2 - 4a} + b/2 \\ \tau_2 = b - \sqrt{b^2 - 4a}/2 \end{cases} \tag{4}$$

Then, $c = R_1 + R_2 + R_0$, $d = R_1\tau_2 + R_2\tau_1 + R_0(\tau_1 + \tau_2)$, the values of the remaining parameters can be obtained by combining Eq. 3 as shown in Eq. 5.

$$\begin{cases} R_1 = \left(\tau_1 c + \tau_2 R_0 - d\right)/\left(\tau_1 - \tau_2\right) \\ R_2 = c - R_1 - R_0 \\ C_1 = \tau_1/R_1 \\ C_2 = \tau_2/R_2 \end{cases} \tag{5}$$

Therefore, Eqs. 4 and 5 are the values of each parameter in the equivalent circuit model.

Adaptive square root unscented Kalman algorithm

The adaptive square root unscented Kalman filter algorithm is based on the unscented Kalman filter algorithm and introduces the idea of an adaptive algorithm and square root filter. It can correct the errors caused by time-varying noise, in addition to improving the numerical instability of the unscented Kalman filter algorithm.

ASRUKF utilizes three linear algebra techniques for square root covariance updating and propagation: QR decomposition (QR), Cholesky factor updating (cholupdate), and effective least squares. The specific calculation process is as follows.

Step 1. Initialize the vector x; the covariance P_o is obtained from the initial value x_0. The initial value of the square root S_0 is obtained from P_0. The square root of the covariance S_k is used in the UT transform instead of P_k. The unscented Kalman filter algorithm steps are involved in the recursive computation.

$$\begin{cases} x_0 = E\left(x_0\right) \\ S_0 = chol\left\{P_0\right\} = chol\left\{\left[\left(x_0 - x_0\right)^T\left(x_0 - x_0\right)\right]\right\} \end{cases} \tag{6}$$

Step 2. The UT transform is then used to find the Sigma point.

$$X_k = \left[x_k\ x_k + \eta S_k\ x_k - \eta S_k\right] \tag{7}$$

Step 3. Time update after obtaining Sigma points.

$$\begin{cases} X_{k+1|k} = f\left[X_k, u_k\right] \\ x_{k+1}^{-} = \sum_{i=0}^{2n} \omega_m^{(i)} X_{k+1|k}^{(i)} \\ S_{k+1}^{-} = qr\left\{\left[\sqrt{\omega_c^1}\left(X_{1:2n,k+1|k} - x_{k+1}^{-}\right)\sqrt{Q_{k+1}}\right]\right\} \\ S_{k+1}^{-} = Chol\left\{S_{k+1}^{-}, X_{0,k+1|k} - x_{k+1}^{-}, \omega_c^0\right\} \\ Y_{k+1|k} = h\left[X_{k+1|k}\right] \\ y_{k+1}^{-} = \sum_{i=0}^{2n} \omega_m^{(i)} y_{i,k+1|k} \end{cases} \tag{8}$$

The updated state estimate $X_{k+1|k}$ for each Sigma point, the output estimate $Y_{k+1|k}$, the weighted $k+1$ moment's state estimate x_{k+1}^{-}, and output estimate y_{k+1}^{-}, and the root of the covariance S_{k+1}^{-}, are obtained. Since ω_c^0 may be negative during the recursion, the matrix is also ensured to be nonnegative after the QR decomposition. The added equation is shown in Eq. 9.

$$S_{k+1}^{-} = S_{k+1}^{-} \pm \sqrt{\left|\omega_c^0\right|}\left(X_{0,k|k-1} - \hat{x}_{k+1}^{-}\right)\left(X_{0,k|k-1} - \hat{x}_{k+1}^{-}\right)^T \tag{9}$$

Step 4. Update the square root of the covariance of the output residuals $S_{y_{k+1}}$, the mutual covariance of the state estimate and the output estimate $P_{x_{k+1}y_{k+1}}$, the Kalman gain matrix K_{k+1}, the posterior estimate of the state quantities x_{k+1}, and the square root of the co-defense of the state estimate errors S_{k+1}.

$$\begin{cases} S_{y_{k+1}} = qr\left\{\left[\sqrt{\omega_c^1}\left(Y_{1:2n,k+1|k} - y_{k+1}^{-}\right)\sqrt{R_{k+1}}\right]\right\} \\ S_{y_{k+1}} = Chol\left\{S_{y_{k+1}}, y_{0,k+1|k} - y_{k+1}^{-}, \omega_c^0\right\} \\ P_{x_{k+1}y_{k+1}} = \sum_{i=0}^{2n} \omega_c^{(i)}\left[X_{i,k+1|k} - x_{k+1}^{-}\right]\left[y_{i,k+1|k} - y_{k+1}^{-}\right] \\ K_{k+1} = \left(\frac{P_{x_{k+1}y_{k+1}}}{S_{y_{k+1}}^T}\right)/S_{y_{k+1}} \\ x_{k+1|k} = x_{k+1}^{-} + K_{k+1}\left(y_{k+1} - y_{k+1}^{-}\right) \\ U = K_{k+1}S_{y_{k+1}} \\ S_{k+1} = Chol\left\{S_{k+1}^{-}, U, -1\right\} \end{cases} \tag{10}$$

Step 5. Adaptive noise estimation. $\hat{q}_k$ and $\hat{Q}_k$ are the average matrix and variance matrix of process noise, respectively; $\hat{r_k}$ and R_k are the average matrix and variance matrix of measurement noise, respectively.

$$\begin{cases} \hat{q}_k = \frac{1}{k}\left[(k-1)\hat{q}_k + \hat{x}_k - \sum_{i=0}^{2n} W_i^m f\left(x_{k-1|k-1}^i, u_{k-1}\right)\right] \\ \hat{Q}_k = \frac{1}{k}\left[(k-1)\hat{Q}_k + K_k e_k e_k K_k^T + P_{x,k} - \sum_{i=0}^{2n} W_i^c\left[x_{k|k-1}^i - \hat{x}_{k|k-1}^{-}\right]\left[x_{k|k-1}^i - \hat{x}_{k|k-1}^{-}\right]^T\right] \\ \hat{r}_k = \frac{1}{k}\left[(k-1)\hat{r}_k + \hat{y}_k - \sum_{i=0}^{2n} W_i^m f\left(x_{k|k-1}^i, u_k\right)\right] \\ \hat{R}_k = \frac{1}{k}\left[(k-1)\hat{R}_{k-1} + e_k e_k + P_{x,k} - \sum_{i=0}^{2n} W_i^c\left[y_{k|k-1}^i - \hat{y}_{k|k-1}^{-}\right]\left[y_{k|k-1}^i - \hat{y}_{k|k-1}^{-}\right]^T\right] \end{cases} \tag{11}$$

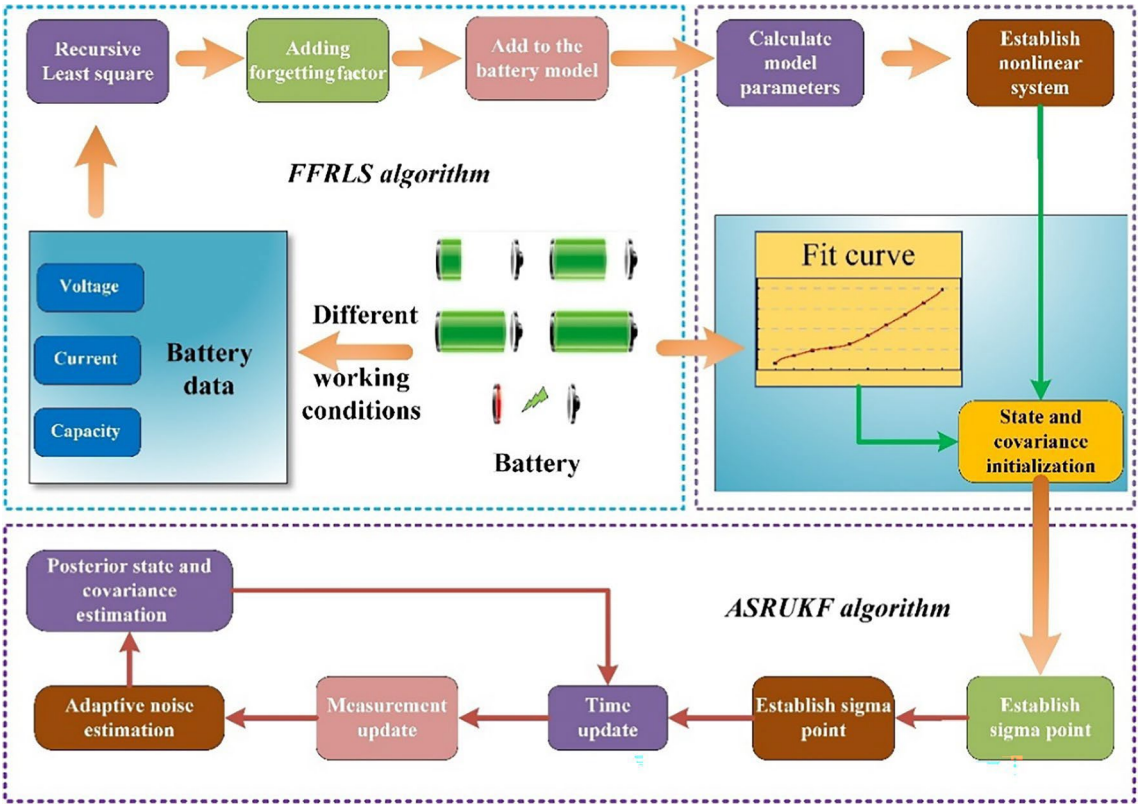

Fig. 2 The structure diagram of the FFRLS-ASRUKF joint algorithm

FFRLS-ASRUKF algorithm

The structure diagram of the FFRLS-ASRUKF joint algorithm is shown in Fig. 2. The least squares parameter identification method with forgetting factor is applied to the parameter identification of the lithium battery equivalent model to identify the parameters in the second-order RC equivalent circuit model. The identified complete parameters are substituted into the adaptive square root unscented Kalman filter algorithm to establish a nonlinear system.

At the same time, according to the current voltage data under three working conditions at different temperatures, the fitting curve of open circuit voltage with SOC and SOE was established, and the fitting curve was input into the adaptive square root unscented Kalman filter algorithm to characterize the current-voltage relationship. All parameters in the ASRUKF algorithm are either calculated based on a second-order circuit model or are rated constant like the battery capacity. Through the above five steps, the adaptive square root unscented Kalman filter derives the SOC and SOE estimates. After the QR decomposition, it also ensures the nonnegativity of the matrix, as it can be negative in the recursive process.

Experimental analysis

Experimental equipment and data sources

An experimental platform is used by the authors to obtain the information of current and voltage of lithium-ion battery under three different working conditions as well as temperatures, as shown in Fig. 3.

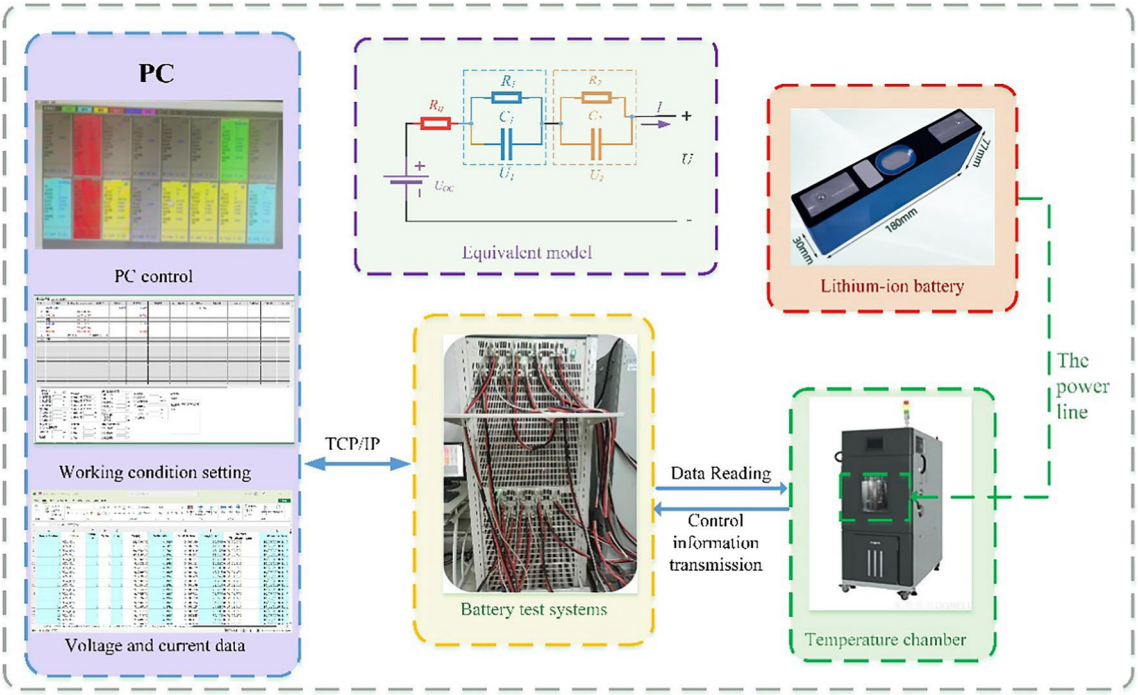

Fig. 3 Schematic of the experimental setup

As shown in Fig. 3, the PC terminal is responsible for set- ting various complex working conditions and recording voltage, current, and other information. The charge/discharge tester controls the charge/discharge detection of the battery, and data is transmitted between the two via TCP/IP protocol. The constant temperature box is connected to the lithium-ion battery and the charge/discharge tester via the power cable and is used to ensure that the temperature of the lithium-ion battery test environment is kept constant at 25, 15, and 5 °C.

The lithium-ion battery used for all the experiments was a single lithium ternary battery manufactured by CATL (Contemporary Amperex Technology Co., Limited) with a model number of 3.7v70Ah. It has a rated voltage of 3.7 V, a rated capacity of 70 Ah, and an internal resistance of 0.7 mΩ. The lithium ternary battery used in this experiment is nickel–cobalt–manganese lithium ternary battery, specifically NCM811, which is composed of nickel (Ni), cobalt (Co), and manganese (Mn). The number indicates the ratio of nickel, cobalt, and manganese; NCM811 means the ratio of nickel, cobalt, and manganese is 8 : 1 : 1. We completed the capacity calibration of the NCM811 battery and measured the initial capacity, i.e., the actual capacity, to be 69.286247 Ah.

The three working conditions are HPPC (hybrid pulse power characteristic), DST (dynamic stress test), and BBDST (Beijing bus dynamic stress test).

HPPC test

(1) Charge the battery with constant current and constant voltage (4.2 V/1C) until it is fully charged.
(2) Let the battery stand for 40 min, and measure and record the terminal voltage of the battery.
(3) Perform current pulse experiments. First, the battery is discharged at a constant current of 1C for 10 s, next left for 40 s, then charged at a constant current of 1 C for 10 s to recover the battery power.
(4) Decrease the battery power by 10% with a constant dis- charge current of 1 C for 6 min, then left for 40 min, and record the terminal voltage as the OCV at this time.
(5) Repeat steps (3) and (4) 10 times until the battery power is 0.

DST test

(1) Charging the battery with a constant current-constant voltage method using a 1 C current, the cut-off voltage and current are 4.2 V and 0.05 C, respectively.

(2) The battery is relaxed for 30 min.
(3) The battery is discharged with a constant current of 0.5 C for 4 min and then relaxed for 30 s.
(4) Charging the battery with a 0.5 C constant current for 2 min and then relaxing for 30 s.
(5) The battery is discharged with a constant current of 1 C for 4 min.
(6) Steps (4) to (5) are repeated until the battery terminal voltage is 2.75 V.

BBDST

The ternary lithium battery is tested by setting up the operating condition experiment by referring to the Beijing bus dynamic stress test. The working condition of the BBDST includes starting, acceleration, sliding, braking, and rapid acceleration. The working time of a complete BBDST is 300 s, which is a small cycle, and its detailed process is shown in Table 1 in Reference [42]. In this paper, many small cycles are performed on the battery to form a BBDST working condition.

Table 1 Error indicators for estimating SOC using various algorithms under HPPC working condition at different temperatures

Algorithm	Temperature (°C)	RMSE ($\times 10^{-2}$)	MAE ($\times 10^{-2}$)	MAPE (%)
ASRUKF	5	0.16	0.12	0.43
	15	0.078	0.003	0.008
	25	0.087	0.050	0.150
SRUKF	5	0.43	0.40	1.46
	15	0.78	0.67	2.39
	25	0.33	0.27	0.94
UKF	5	0.95	0.77	3.44
	15	0.95	0.82	2.56
	25	0.63	0.51	1.53
EKF	5	1.22	0.97	4.29
	15	1.02	0.91	2.72
	25	0.71	0.58	1.83

FFRLS under different working conditions

Taking 25°C as an example, the voltage and error plots for FFRLS parameter identification under three working conditions are shown in Fig. 4.

As shown in Fig. 4, the voltages identified by FFRLS for the three operating conditions are very close to the actual voltages, and this feature does not change with increasing time. It can be seen that the forgetting factor recursive least squares method can effectively simulate the internal model of lithium batteries, with a simulation error of only 0.0336 V or less for voltage. Meanwhile, the voltage error at the later stage of parameter identification is larger than that at the earlier stage of parameter identification, which is mainly due to the instability at the later stage of discharge caused by the nonlinearity of the lithium-ion battery, which is an uncontrollable factor.

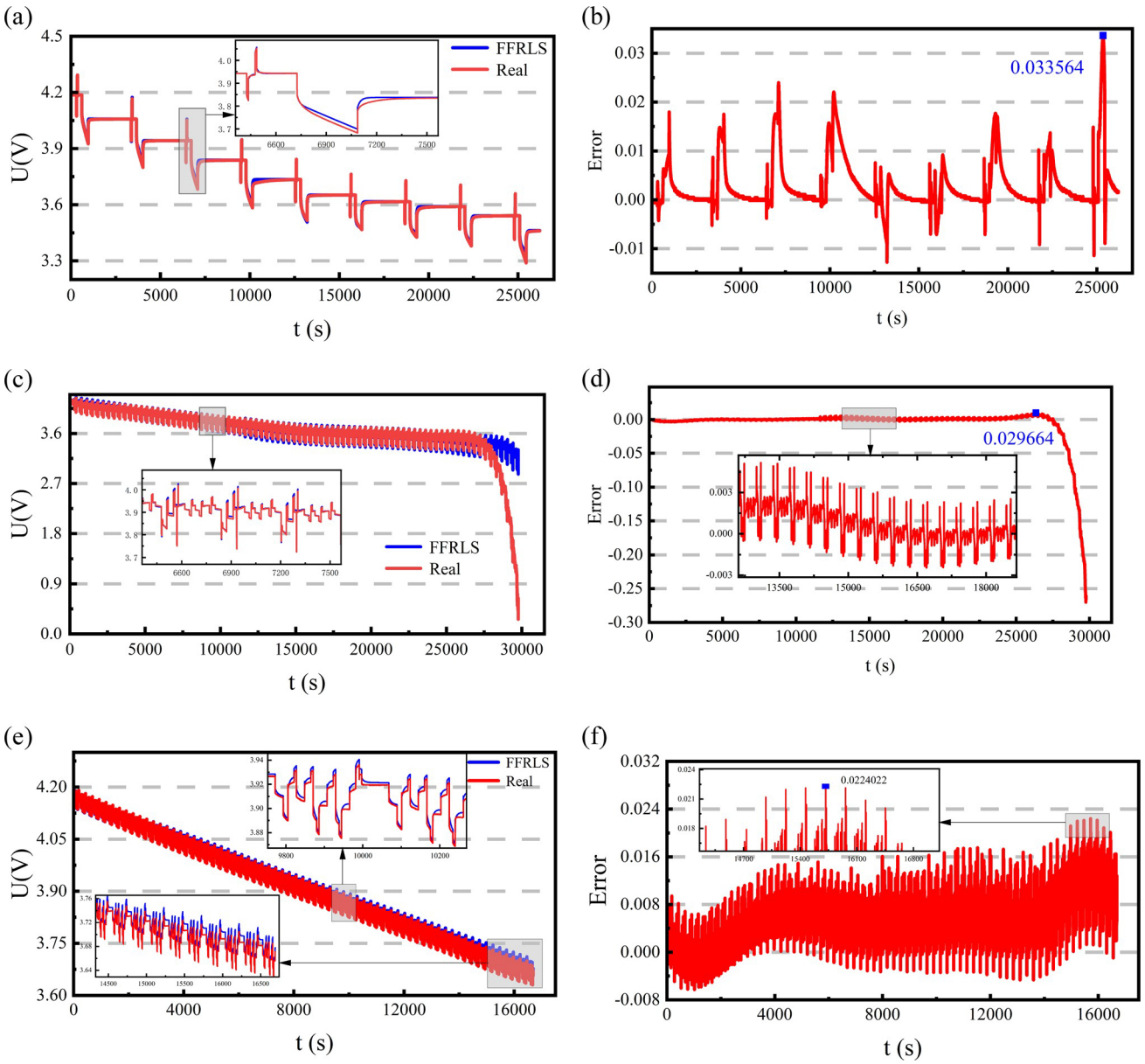

Fig. 4 Voltage and error diagrams of lithium-ion batteries under three operating conditions at 25 °C. **a**, **c**, **e.** The voltage simulation plots of HPPC, DST, and BBDST, respectively. **b**, **d**, **f.** The identification error plots for HPPC, DST, and BBDST, respectively.

Parameter settings

Before using each algorithm for the prediction of SOC and SOE, the parameters need to be set initially, including the setting of the covariance matrix P, process noise matrix Q, and measurement noise R. The smaller the Q value, the easier the system is to converge, and the higher our trust in the predicted values of the model. But if Q is too small, the system is prone to divergence. If Q is zero, then we only trust the predicted value. The higher the Q value, the lower our trust in predictions, and the higher our trust in measured values. If the Q value is infinite, then we only trust the measured value. The size of R is also important: if R is too large, the Kalman filter response will slow down because it reduces its trust in newly measured values. The smaller the R, the faster the system converges, but if it is too small, it is prone to oscillations.

The test can be started by adjusting Q from small to large and R from large to small, fixing one value to adjust the other first. In this paper, the method used for parameter setting is to fix the value of R first and then adjust the value of Q. Since the error of the current sensor and voltage sensor can be determined as a smaller value through a large number of experiments and experience, R can be set

as a smaller value first, which is set to 0.01 in this paper. And since all the experiments were conducted in the same equipment and the same model, and the batteries used were fully rested at the beginning of each start of the experiment, the internal dynamic and static responses of the batteries tend to be stabilized, so Q can also be set to a smaller value first.

There is another key value in the system, P, which is the initial value of the error covariance, which indicates our confidence in the current prediction state; the smaller it is, the more we believe in the current prediction state. Since the prediction accuracy of the second-order circuit model is relatively high, the value of P can be initially set smaller. As the Kalman filtering iterates, the value of P will keep changing; when the system enters the steady state, the value of P will converge to a minimum estimate of the variance matrix, and the Kalman gain is also optimal at that time, so this value only affects the initial convergence speed.

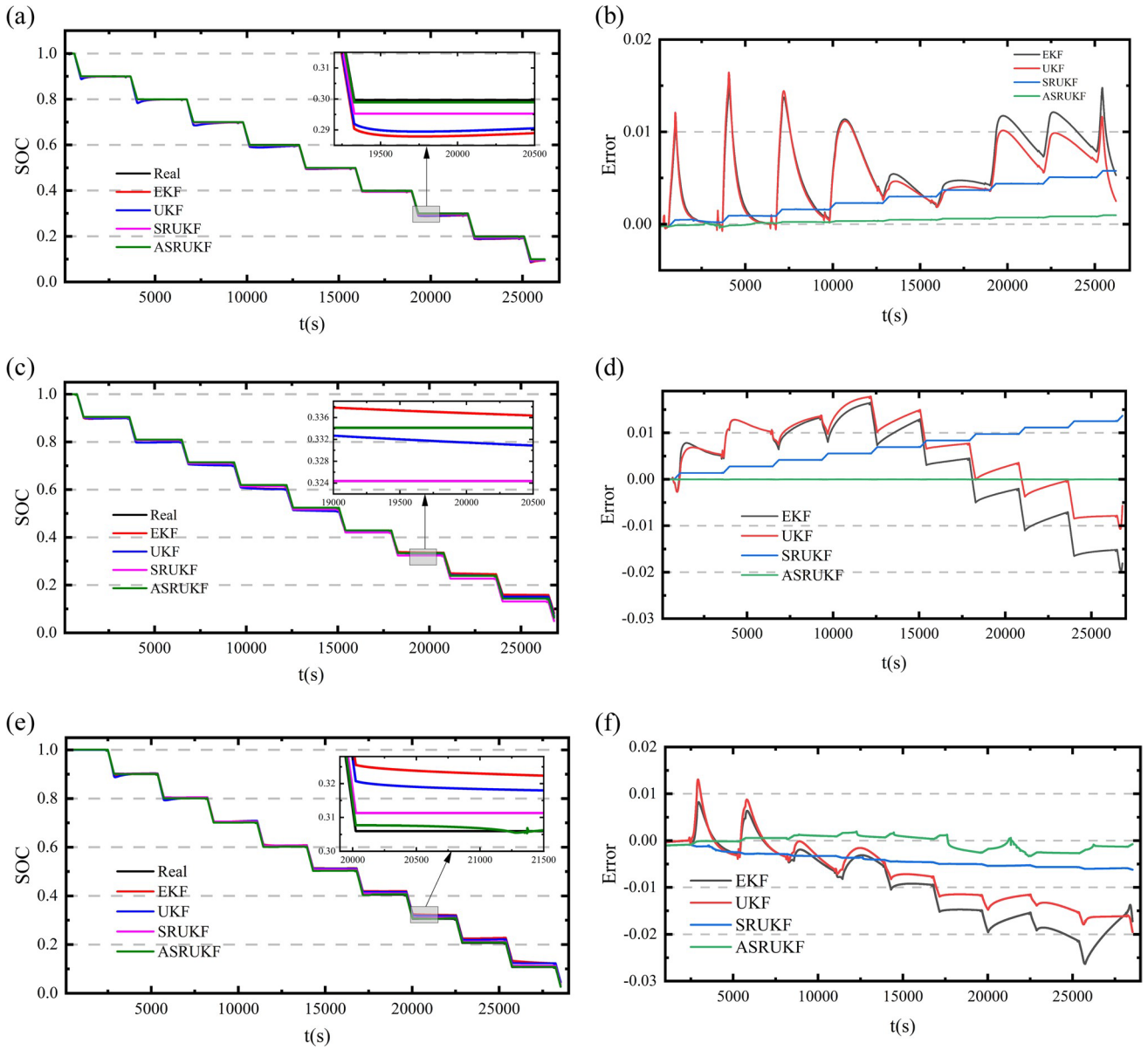

Fig. 5 SOC estimation results at different temperatures under HPPC working condition. **a**, **c**, **e.** The SOC estimation plots for 25, 15, and 5 °C, respectively. **b**, **d**, **f.** The plots of the SOC estimation errors for 25, 15, and 5 °C, respectively.

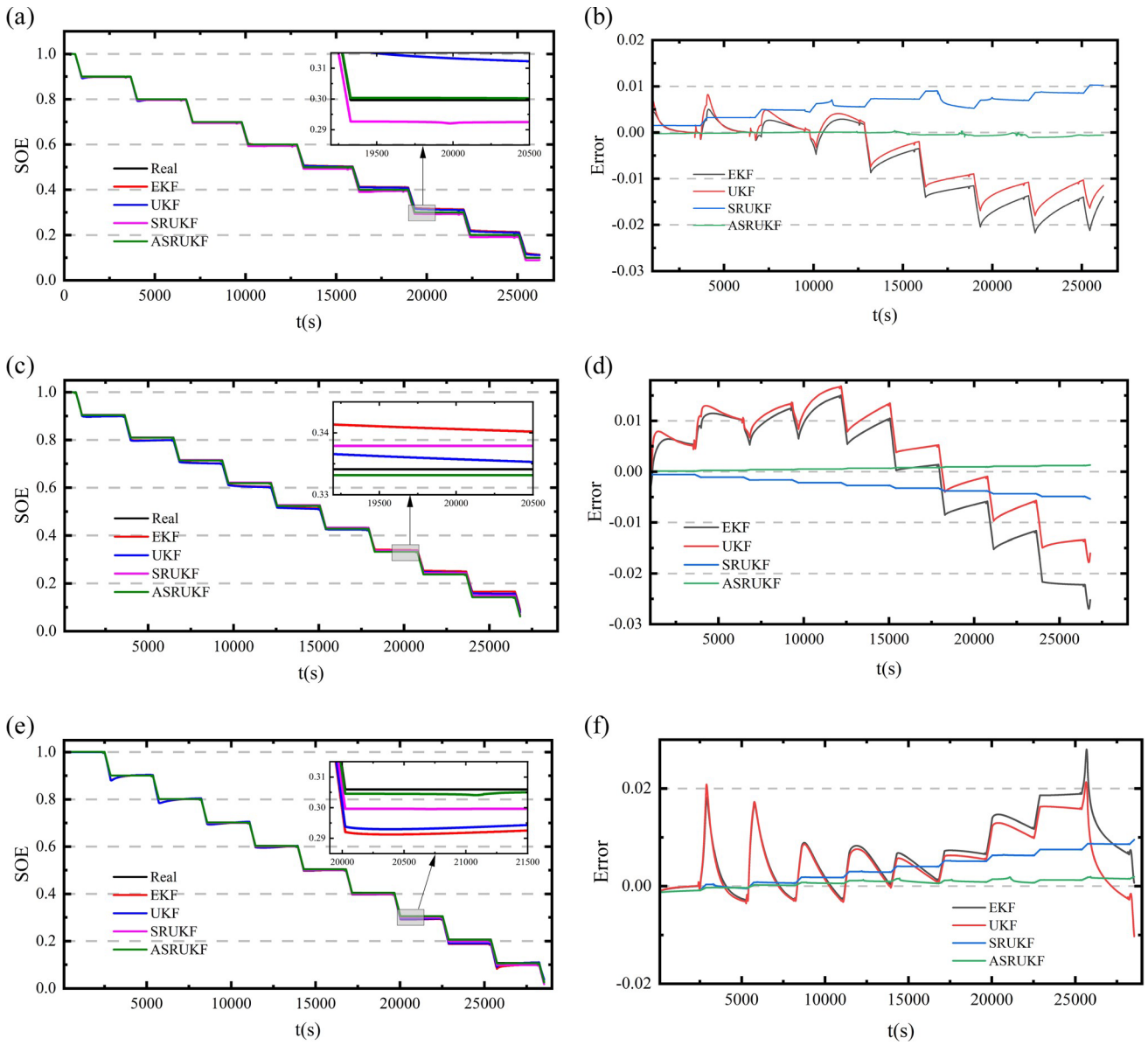

Fig. 6 SOE estimation results at different temperatures under HPPC working condition. **a**, **c**, **e.** The SOE estimation plots for 25, 15, and 5 °C , respectively. **b**, **d**, **f.** The plots of the SOE estimation errors for 25, 15, and 5 °C, respectively.

Predictive validation under HPPC working condition

To verify the feasibility of the forgetting factor recursive least square-adaptive square root unscented Kalman filter algorithm for SOC and SOE estimations of lithium-ion batteries, an estimation model for SOC and SOE of lithium-ion batteries is constructed. The prediction results of SOC and SOE of lithium-ion batteries under HPPC operating conditions at 25, 15, and 5 °C are plotted in Figs. 5 and 6, which are compared with ASRUKF, UKF, and EKF algorithms in order to analyze and compare the prediction performance of ASRUKF at different temperatures.

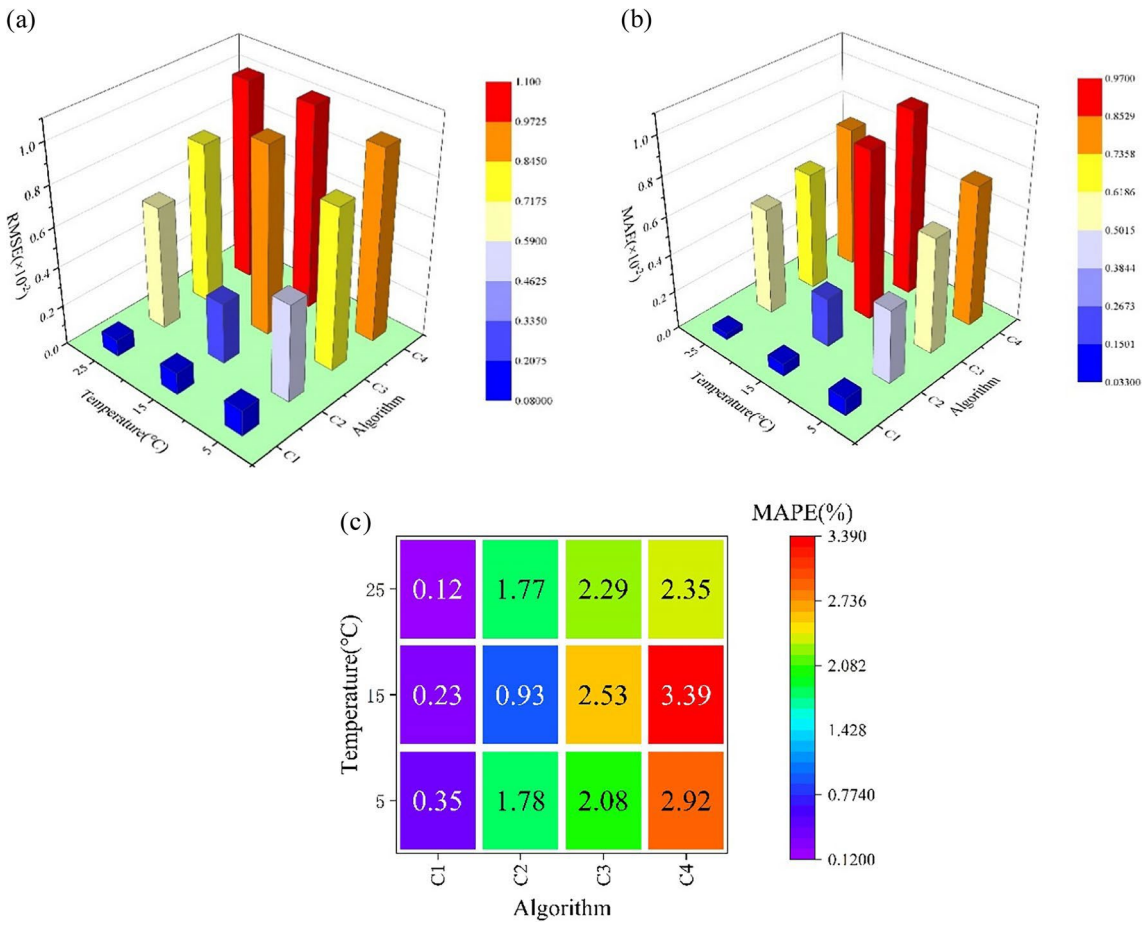

Fig. 7 Error indicators for estimating SOE using various algorithms under HPPC working condition at different temperatures. **a**–**c** RMSE, MAE, and MAPE, respectively; C1~C4 represent ASRUKF, SRUKF, UKF, and EKF, respectively.

Through the error indicators of the final result, including root mean square error (RMSE), mean absolute error (MAE), and mean absolute percentage error (MAPE), the predictive effect of SOC and SOE can be displayed more intuitively. The formula is as follows:

$$\begin{cases} \mathrm{RMSE} = \sqrt{\frac{1}{n}\sum_{i=1}^{n}\left(\hat{y}_i - y_i\right)^2} \\ \mathrm{MAE} = \frac{1}{n}\sum_{i=1}^{n}\left|\hat{y}_i - y_i\right| \\ \mathrm{MAPE} = \frac{1}{n}\sum_{i=1}^{n}\left|\frac{\hat{y}_i - y_i}{y_i}\right| \times 100\% \end{cases} \tag{12}$$

Among them, $\hat{y}$ represents the predicted value, and y rep- resents the true value. The MAE, MAPE, and RMSE of SOC estimation at different temperatures under HPPC condition are shown in Table 1. And The MAE, MAPE, and RMSE of SOE estimation at different temperatures under HPPC condition are shown in Fig. 7.

From Figs. 5 and 6, it can be seen that ASRUKF can effectively estimate the SOC and SOE of lithium-ion batteries at different temperatures, and its effectiveness is significantly better than that of SRUKF, UKF, and EKF. ASRUKF has high accuracy and convergence, making it suitable for predicting SOC and SOE. Table 1 shows that the error index of ASRUKF for predicting SOC is superior to SRUKF, UKF, and EKF at all temperatures.

Under HPPC condition, ASRUKF has the best estimation effect at 15 °C. At low temperatures of 5 °C, ASRUKF has a relatively weak estimation effect on SOC, but the RMSE, MAE, and MAPE do not exceed 0.0016, 0.0012, and 0.43%. Figure 7 shows the error indicators of each algorithm at different temperatures under HPPC condition. All four algorithms can effectively estimate the SOE, with ASRUKF having the best performance, RMSE and MAE not exceeding 0.002, MAPE not exceeding 0.35%, and its estimation performance at 25 °C being the best.

Predictive validation under DST working condition

To verify the performance of FFLRS-ASRUKF under different working conditions, the SOC and SOE estimation results at different temperatures under DST working condition are shown in Figs. 8 and 9.

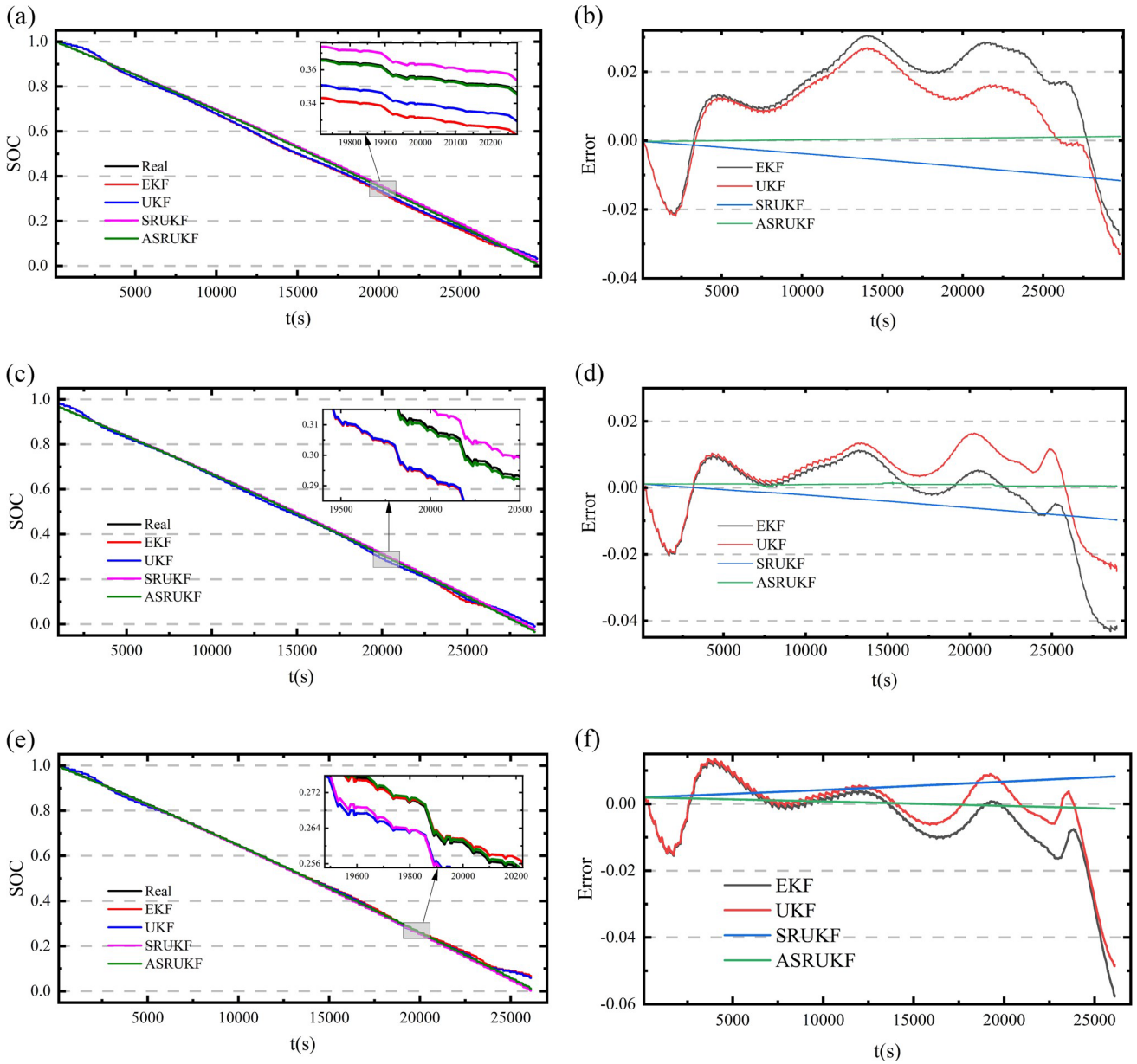

Fig. 8 SOC estimation results at different temperatures under DST working condition. **a**, **c**, **e.** The SOC estimation plots for 25, 15, and 5 °C, respectively. **b**, **d**, **f.** The plots of the SOC estimation errors for 25, 15, and 5 °C, respectively.

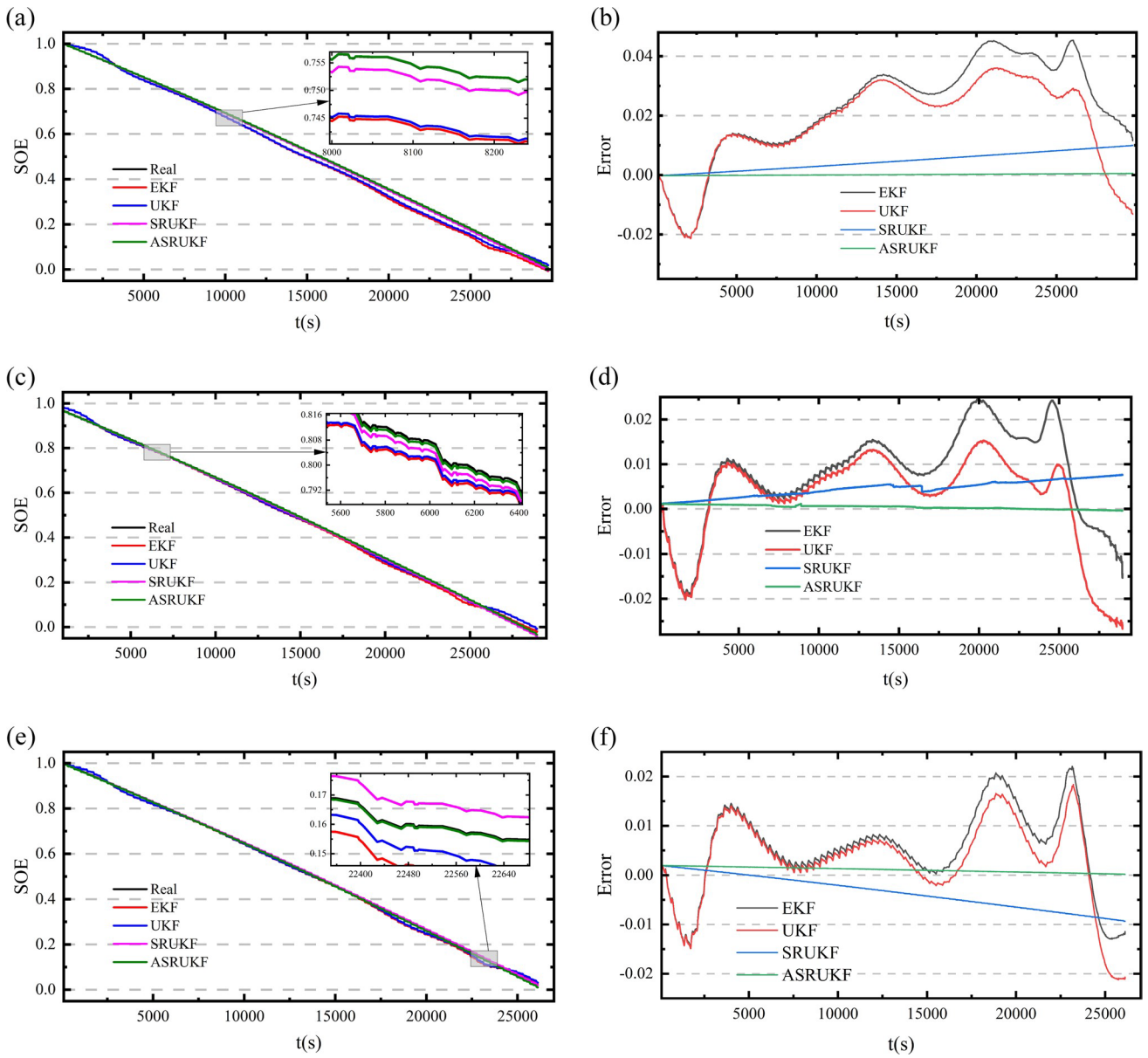

Fig. 9 SOE estimation results at different temperatures under DST working condition. **a**, **c**, **e** The SOE estimation plots for 25, 15, and 5 °C, respectively. **b**, **d**, **f** The plots of the SOE estimation errors for 25, 15, and 5 °C, respectively

The MAE, MAPE, and RMSE of SOC estimation at different temperatures under DST working condition are shown in Table 2. And the MAE, MAPE, and RMSE of SOE estimation at different temperatures under DST working condition are shown in Fig. 10.

As shown in Figs. 8 and 9, ASRUKF can accurately estimate the SOC and SOE of lithium-ion batteries at three different temperatures under DST working condition, similarly as under HPPC. Unlike UKF and EKF, ASRUKF can ensure convergence and stability on a more accurate basis than ASRUKF estimation. Table 2 shows the error indicators of the estimated SOC for each algorithm at different temperatures under DST conditions. Among them, ASRUKF is significantly superior to other algorithms at three temperatures, with RMSE, MAE, and MAPE not exceeding 0.0013, 0.0009, and 0.70%, respectively. From Fig. 10, it can be seen that all four algorithms can estimate the SOE of lithium-ion batteries under DST working condition to some extent, but ASRUKF has the best estimation effect and responds effectively to the SOE of lithium-ion batteries at both low and ambient temperatures.

Predictive validation under BBDST working condition

Figures 11 and 12 show the results of different algorithms for estimating the SOC and SOE of lithium-ion batteries at different temperatures under BBDST working condition.

The MAE, MAPE, and RMSE of SOC estimation at different temperatures under BBDST working condition are shown in Table 3. And the MAE, MAPE, and RMSE of SOE estimation at different temperatures under BBDST working condition are shown in Fig. 13.

From Figs. 11 and 12, it can be seen that ASRUKF still has significant advantages under BBDST working condition, as it can fit the original curves of SOC and SOE almost perfectly, with small errors and convergence. As can be seen from Table 3 and Fig. 13, the algorithms perform best at 15 °C and are relatively weak at low temperatures of 5 °C under BBDST working condition. Similarly, ASRUKF outperforms the other algorithms regardless of temperature, keeping the RMSE, MAE, and MAPE within 0.0016, 0.0009, and 0.71%, respectively.

Table 2 Error indicators for estimating SOC using various algorithms under DST working condition at different temperatures

Algorithm	Temperature (°C)	RMSE ($\times 10^{-2}$)	MAE ($\times 10^{-2}$)	MAPE (%)
ASRUKF	5	0.13	0.09	0.41
	15	0.09	0.05	0.70
	25	0.08	0.05	0.28
SRUKF	5	0.54	0.50	2.88
	15	0.49	0.45	3.01
	25	0.40	0.33	2.72
UKF	5	0.91	0.72	5.18
	15	1.08	0.91	8.52
	25	0.92	0.83	3.54
EKF	5	1.07	0.67	7.94
	15	1.28	1.12	9.43
	25	1.102	0.85	4.31

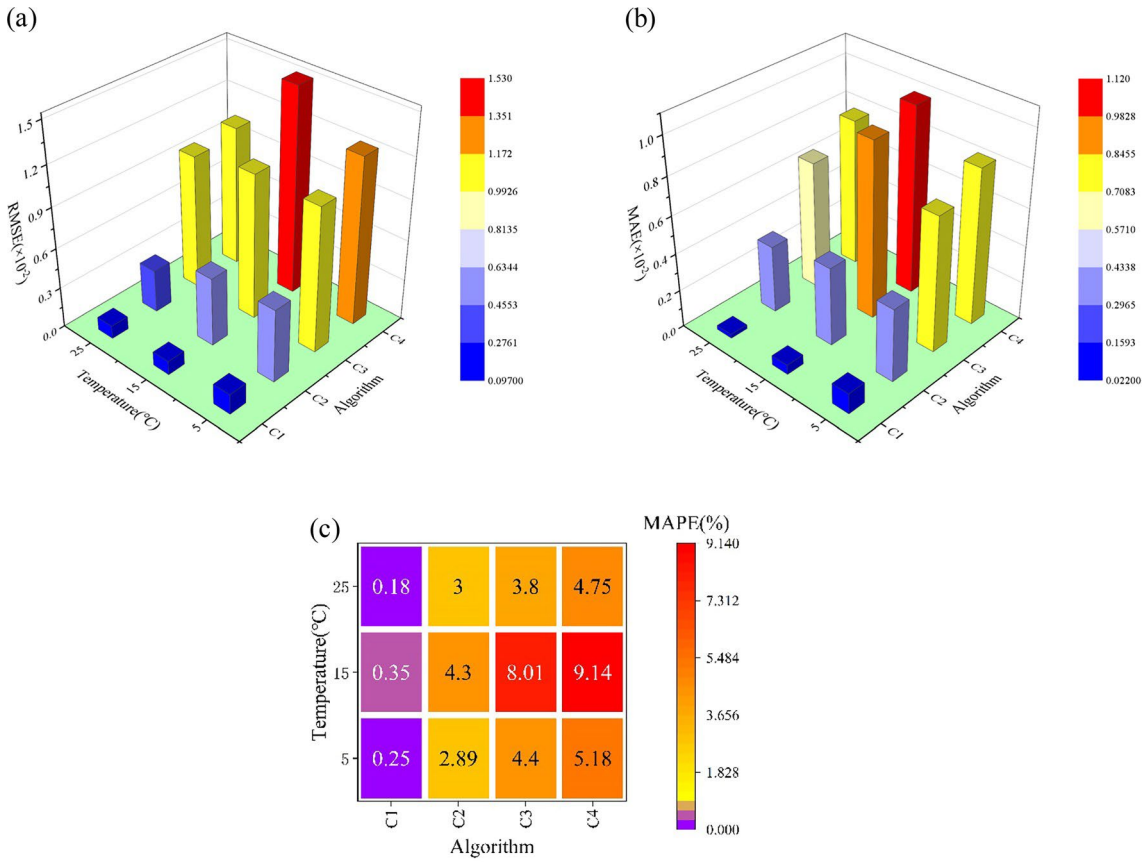

Fig. 10 Error indicators for estimating SOE using various algorithms under DST working condition at different temperatures. **a**–**c** RMSE, MAE, and MAPE, respectively; C1~C4 represent ASRUKF, SRUKF, UKF, and EKF, respectively.

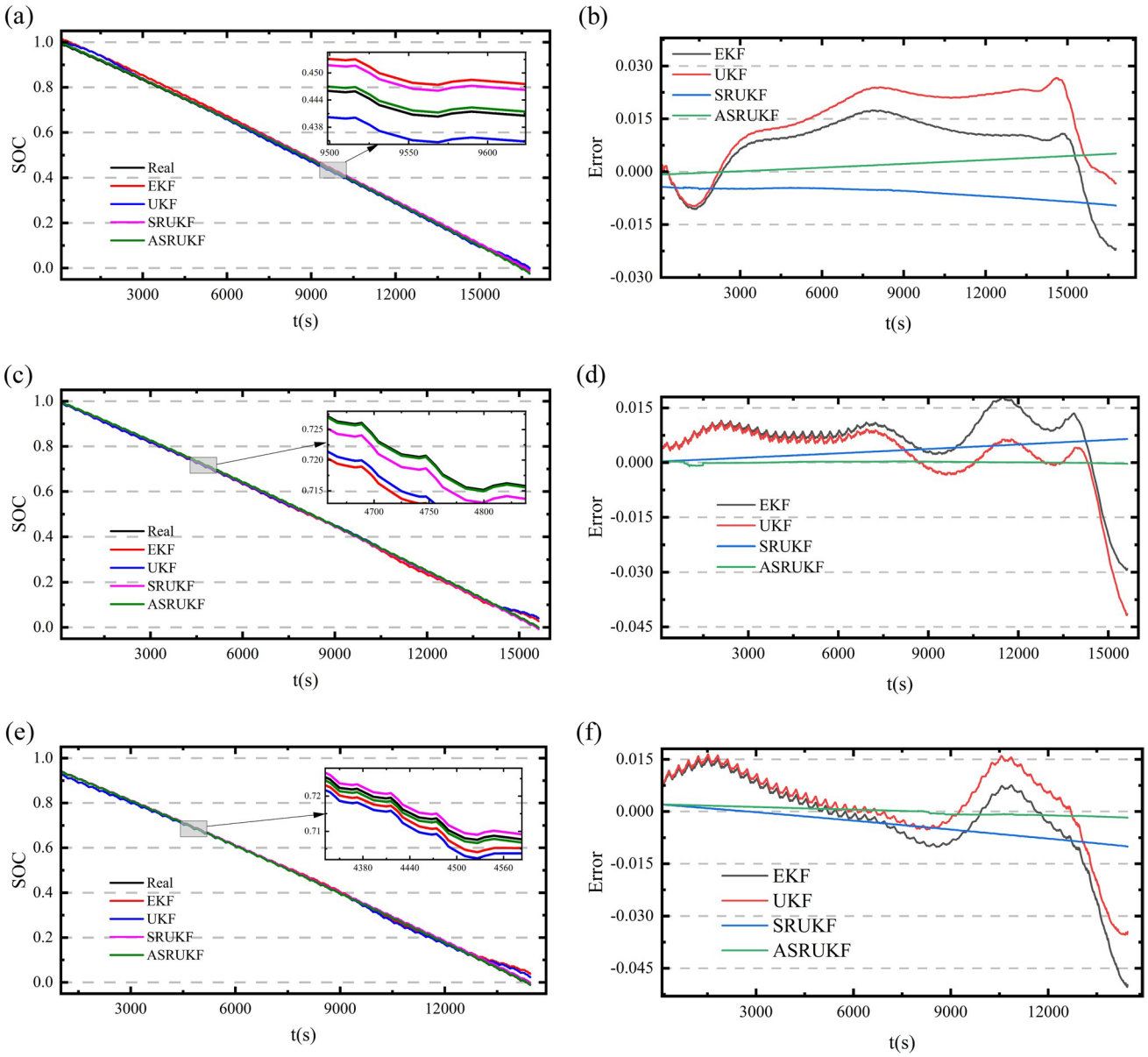

Fig. 11 SOC estimation results at different temperatures under BBDST working condition. **a**, **c**, **e** The SOC estimation plots for 25, 15, and 5 °C, respectively. **b**, **d**, **f** The plots of the SOC estimation errors for 25, 15, and 5 °C, respectively

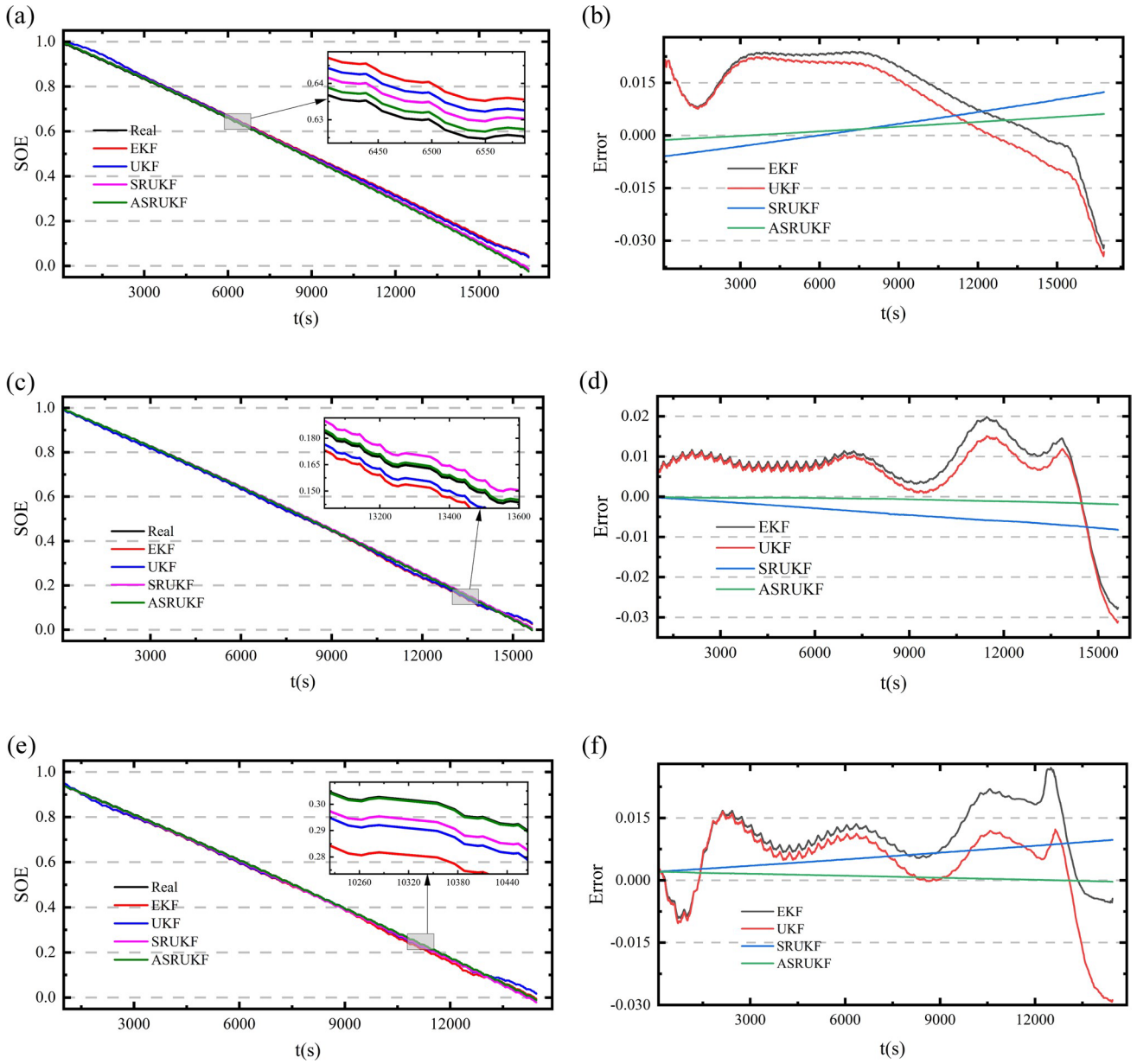

Fig. 12 SOE estimation results at different temperatures under BBDST working condition. **a**, **c**, **e** The SOE estimation plots for 25, 15, and 5 °C, respectively. **b**, **d**, **f** The plots of the SOE estimation errors for 25, 15, and 5 °C, respectively

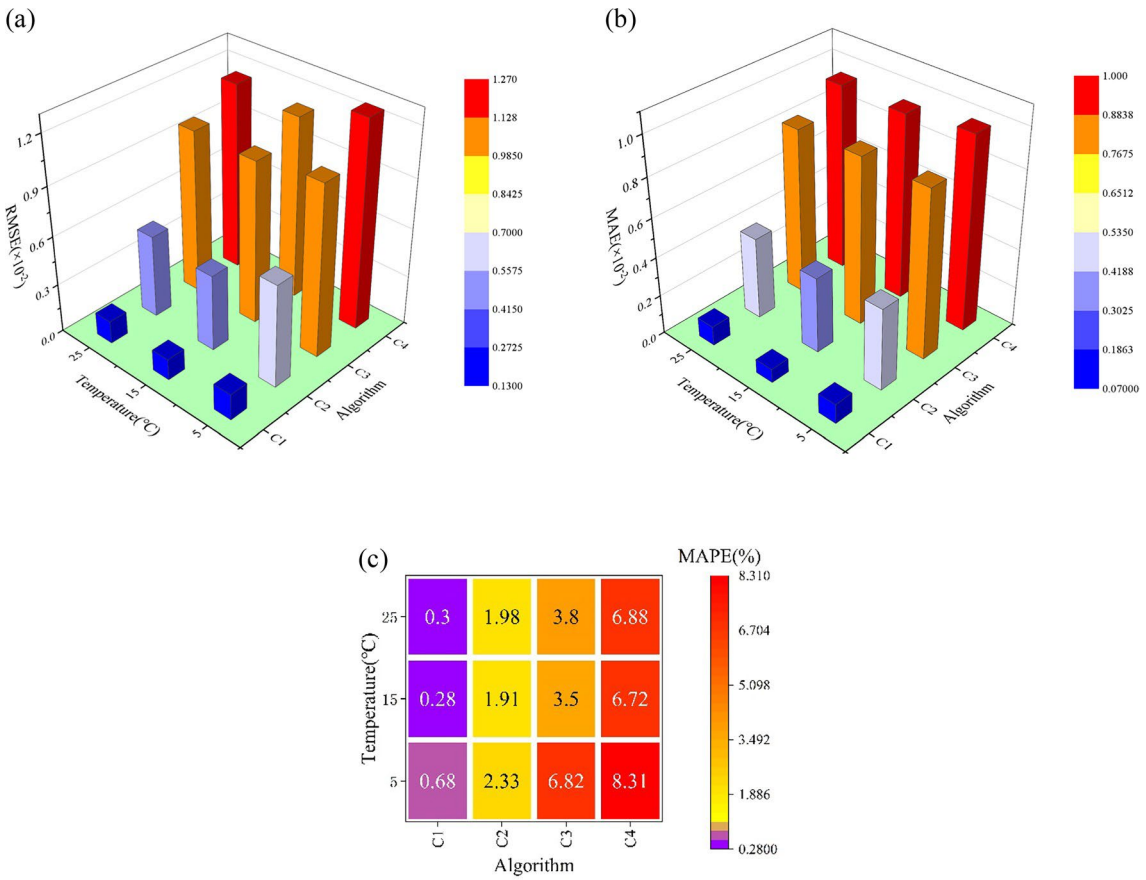

Fig. 13 Error indicators for estimating SOE using various algorithms under BBDST working condition at different temperatures. **a–c** RMSE, MAE, and MAPE, respectively; C1~C4 represent ASRUKF, SRUKF, UKF, and EKF, respectively.

Table 3 Error indicators for estimating SOC using various algorithms under BBDST working condition at different temperatures

Algorithm	Temperature (°C)	RMSE ($\times 10^{-2}$)	MAE ($\times 10^{-2}$)	MAPE (%)
ASRUKF	5	0.16	0.09	0.71
	15	0.10	0.02	0.26
	25	0.12	0.05	0.31
SRUKF	5	0.63	0.57	2.01
	15	0.39	0.33	1.83
	25	0.42	0.38	0.93
UKF	5	1.05	0.86	6.825
	15	0.95	0.66	3.4
	25	0.96	0.68	3.59
EKF	5	1.27	1.12	9.41
	15	1.07	0.94	6.49
	25	1.11	1.02	7.58

Predictive validation after adding current offset

In order to verify the robustness of the FFRLS-ASRUKF algorithm, current offsets of + 1 A and – 1 A were added to the battery measurement data to treat them as disturbances. From the above, it can be seen that both SOC and SOE predictions of ASRUKF are relatively worst under BBDST working condition at 5 °C. To test the robustness of the algorithm, a current offset is added in the worst case environment. The prediction results of SOC and SOE are plotted in Figs. 14 and 15 for the BBDST condition at 5 °C.

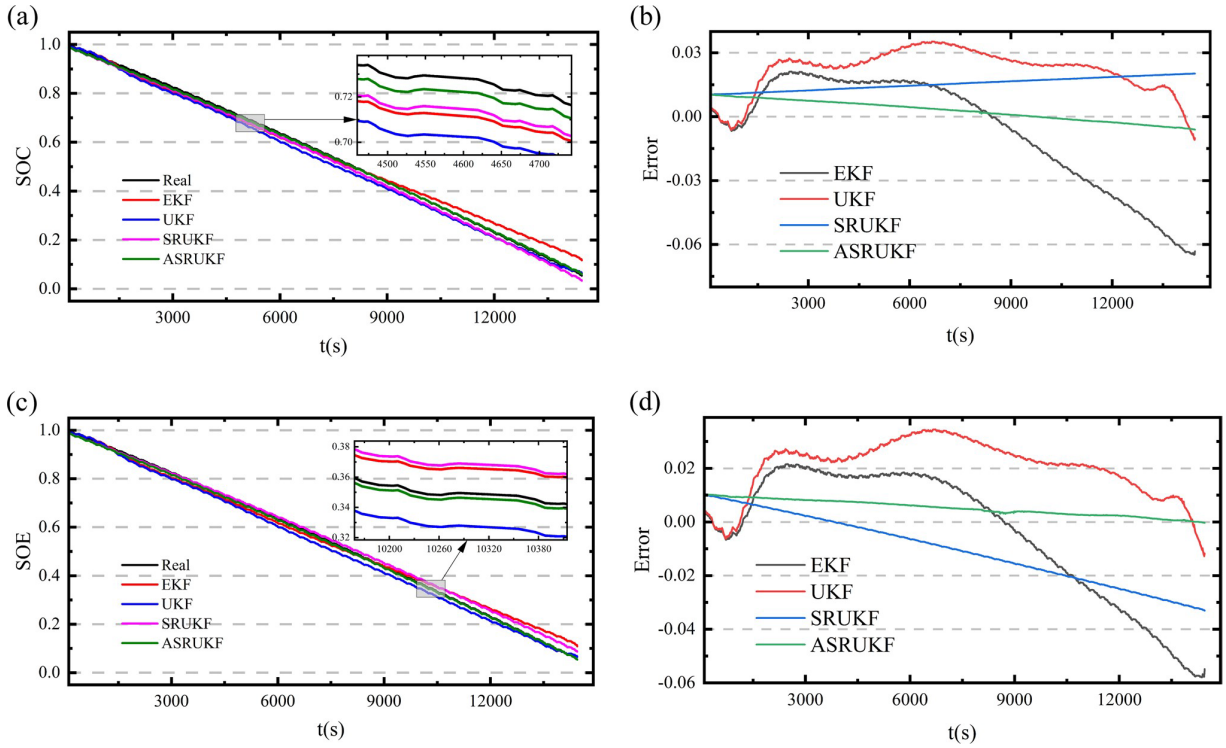

Fig. 14 SOC and SOE prediction results for current offset + 1 A. **a**, **c.** Plots of prediction results for SOC and SOE, respectively. **b**, **d.** Plots of prediction errors for SOC and SOE, respectively.

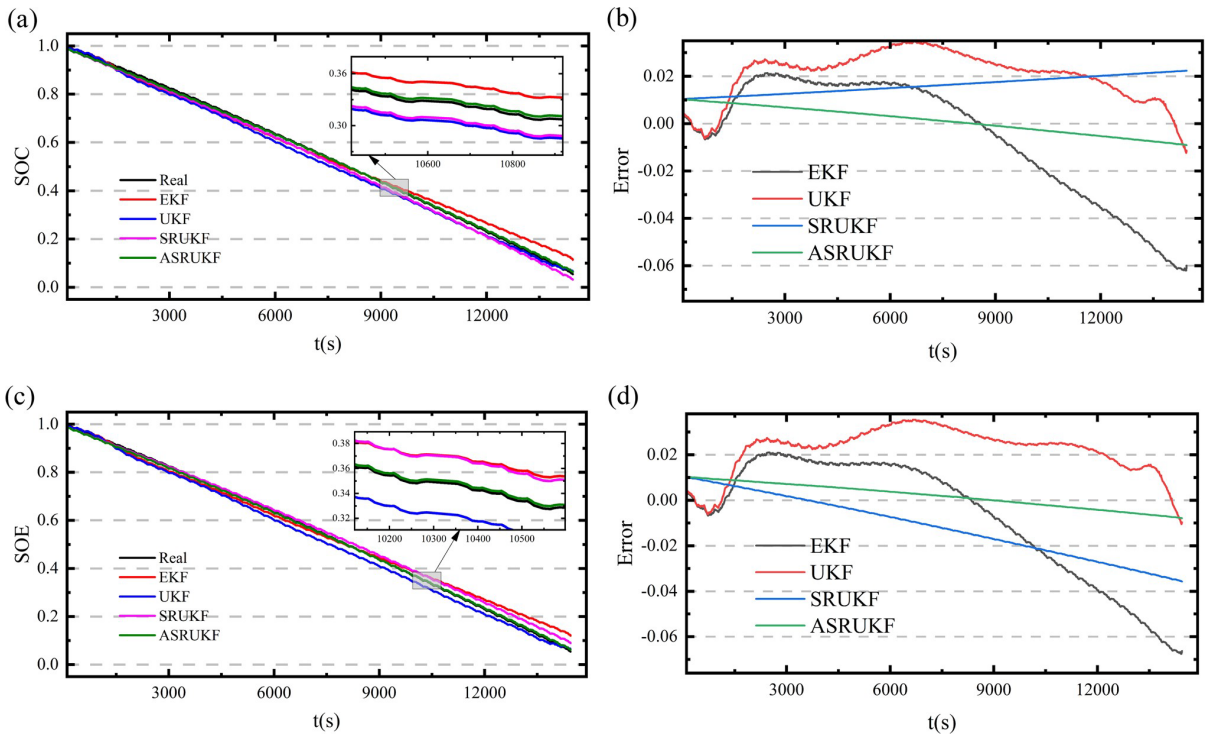

Fig. 15 SOC and SOE prediction results for current offset – 1 A. **a**, **c.** Plots of prediction results for SOC and SOE, respectively. **b**, **d.** Plots of prediction errors for SOC and SOE, respectively.

The error metrics for each algorithm after current offsets of + 1 A and – 1 A are shown in Table 4.

Table 4 Error metrics for each algorithm after current offsets of + 1 A and – 1 A

Algorithm	Current offset (A)	Projected projects	RMSE ($\times 10^{-2}$)	MAE ($\times 10^{-2}$)	MAPE (%)
ASRUKF	+ 1	SOC	0.55	0.46	1.19
		SOE	0.61	0.53	0.91
	− 1	SOC	0.58	0.50	1.62
		SOE	0.57	0.48	1.43
SRUKF	+ 1	SOC	1.56	1.53	5.05
		SOE	1.63	1.32	6.01
	− 1	SOC	1.65	1.61	5.43
		SOE	1.77	1.43	6.53
UKF	+ 1	SOC	2.40	2.22	5.34
		SOE	2.28	2.08	4.79
	− 1	SOC	2.31	2.11	4.90
		SOE	2.43	2.25	5.44
EKF	+ 1	SOC	2.64	2.09	9.97
		SOE	2.42	1.97	9.04
	− 1	SOC	2.55	2.04	9.60
		SOE	2.73	2.14	10.35

According to Figs. 14 and 15 and Table 4, and in combination with the above, it can be seen that ASRUKF can still accurately estimate SOC and SOE after being affected by the current offset, and although the values of RMSE, MAE, and MAPE have increased to a certain extent, the prediction effect of ASRUKF can still satisfy the needs of normal operation of lithium-ion batteries.

Conclusion

State of charge and state of energy are important battery health parameters which have a bearing on whether the battery management system can control the battery effectively. This study proposes an FFRLS-ASRUKF method for collaborative estimation of state of charge and state of energy of lithium-ion batteries based on the ASRUKF algorithm through the construction of a second-order equivalent circuit model. FFRLS is used for online identification of parameters in battery model, and an adaptive link is added to SRUKF to improve the convergence and prediction accuracy of the algorithm to compensate for the shortcomings of EKF and UKF. Experimental results show that FFRLS can effectively simulate lithium-ion battery internal changes. At 25 °C, the maximum voltage identification error in HPPC, DST, and BBDST working conditions does not exceed 0.0336, 0.0297, and 0.0225 V, respectively. After FFRLS identification, each parameter is input to each algorithm to estimate the SOC and SOE of lithium-ion batteries. To verify the superiority of FFRLS-ASRUKF, experimental verification was performed at different temperatures of HPPC, DST, and BBDST. And the robustness of ASRUKF has been verified by adding current offsets at temperatures and operating conditions where ASRUKF performs the worst. The experimental results show that under HPPC working condition, ASRUKF has the best estimation effect of SOC at 15 °C, with RMSE, MAE, and MAPE not exceeding 0.0008, 0.0003, and 0.08%, respectively. The estimation effect of SOE is the best at 25 °C, with RMSE, MAE, and MAPE not exceeding 0.0009, 0.0004, and 0.12%, respectively. Under DST working condition, ASRUKF has the best estimation of SOC at 25 °C, with RMSE, MAE, and MAPE not exceeding 0.0008, 0.0005, and 0.28%, respectively. SOE estimation is the best at 25°C, with RMSE, MAE, and MAPE not exceeding 0.001, 0.0003, and 0.18%, respectively. Under BBDST working condition, ASRUKF has the best estimation of SOC at 15 °C, with RMSE, MAE, and MAPE not exceeding 0.0010, 0.0002, and 0.26%, respectively. Estimation of SOE is the best at 15°C with RMSE, MAE, and MAPE not exceeding 0.0013, 0.0007, and 0.28%, respectively. After adding the current offset, ASRUKF is still able to effectively predict the SOC and SOE, and the RMSE, MAE, and MAPE do not exceed 0.0058, 0.0053, and 1.62%, respectively. In summary, the method proposed in this article has high accuracy and good robustness, providing reliable guarantees for the normal operation of electric vehicles and factory equipment.

Author contributions Tao Zhu completed the writing of the paper, and Shunli Wang, Yongcun Fan, Heng Zhou, Yifei Zhou, and Carlos Fernandez reviewed and proposed revisions, and all authors reviewed the manuscript.

Funding The work was supported by the National Natural Science Foundation of China (Nos. 62173281 and 61801407).

References

1. Modi S, Bhattacharya J, Basak P (2021) Convolutional neural network-bagged decision tree: a hybrid approach to reduce electric vehicle's driver's range anxiety by estimating energy consumption in real-time. Soft Comput 25(3):2399–2416
2. Niu Y (2021) Research on the development of new energy vehicles and power lithium batteries. Insight-Energy Sci 3(1):1–4
3. Ge H, Huang J, Zhang JB, Li Z (2016) Temperature-adaptive alternating current preheating of lithium-ion batteries with lithium deposition prevention. J Electrochem Soc 163(2):A290–A2A9
4. Manzetti S, Mariasiu F (2015) Electric vehicle battery technologies: from present state to future systems. Renew Sustain Energy Rev 51:1004–1012
5. Van CN, Vinh TN (2020) Soc estimation of the lithium-ion battery pack using a sigma point Kalman filter based on a cell's second order dynamic model. Appl Sci 10(5):1–17
6. Jiang C, Wang SL, Wu B, Fernandez C, Xiong X, Coffie-Ken J (2021) A state-of-charge estimation method of the power lithium- ion battery in complex conditions based on adaptive square root extended Kalman filter. Energy 219:1–23
7. Nizam M, Mujianto A, Waloyo HT, Purwanto A (2015) Decision tree for state of charge (SOC) prediction of LiFePO4 battery. In: Proceeding joint international conference on electric vehicular technology and industrial, mechanical, electrical, and chemical engineering (ICEVT & IMECE). IEEE, pp 359–361
8. Hannan MA, Lipu MSH, Hussain A, Mohamed A (2017) A review of lithium-ion battery state of charge estimation and management system in electric vehicle applications: challenges and recommendations. Renew Sustain Energy Rev 78:834–854
9. He ZW, Gao MY, Wang CS, Wang LY, Liu YY (2013) Adaptive state of charge estimation for Li-ion batteries based on an unscented Kalman filter with an enhanced battery model. Ener- gies 6(8):4134–4151
10. Xu L, Wang JP, Chen QS (2012) Kalman filtering state of charge estimation for battery management system based on a stochastic fuzzy neural network battery model. Energy Convers Manag 53(1):33–39
11. Rivera-Barrera JP, Munoz-Galeano N, Sarmiento-Maldonado HO (2017) SoC estimation for lithium-ion batteries: review and future challenges. Electronics 6(4):1–34
12. Wei ZB, Zhao JY, Zou CF, Lim TM, Tseng KJ (2018) Comparative study of methods for integrated model identification and state of charge estimation of lithium-ion battery. J Power Sources 402:189–197
13. Sturm J, Ennifar H, Erhard SV, Rheinfeld A, Kosch S, Jossen A (2018) State estimation of lithium-ion cells using a physico-chemical model based extended Kalman filter. Appl Energy 223:103–123
14. Guo N, Fang Y, Tian Z, Cao S (2019) Research on SOC fuzzy weighted algorithm based on GA-BP neural network and ampere integral method. J Eng 2019(15):576–580
15. Zheng YL, He F, Wang WL (2019) A method to identify lithium battery parameters and estimate SOC based on different temperatures and driving conditions. Electronics 8(12):1–15
16. Tian Y, Xia BZ, Sun W, Xu ZH, Zheng WW (2014) A modified model based state of charge estimation of power lithium-ion batteries using unscented Kalman filter. J Power Sources 270:619–626
17. He HW, Qin HZ, Sun XK, Shui YP (2013) Comparison study on the battery SoC estimation with EKF and UKF algorithms. Energies 6(10):5088–5100
18. Yang FF, Zhang SH, Li WH, Miao Q (2020) State-of-charge estimation of lithium-ion batteries using LSTM and UKF. Energy 201:1–37
19. Wang X, SunQ Chen L, Mu D, Liu R (2022) Mixture maximum correntropy criterion unscented Kalman filter for robust SOC estimation. In 2022 IEEE 5th International Conference on Electronic Information and Communication Technology (ICEICT). Hefei, China, pp 670–676
20. Wang WD, Wang XT, Xiang CL, Wei C, Zhao YL (2018) Unscented Kalman filter-based battery SOC estimation and peak power prediction method for power distribution of hybrid electric vehicles. Ieee Access 6:35957–35965
21. Van der Merwe R, Wan EA (2001) The square-root unscented Kalman filter for state and parameter-estimation. In 2001 IEEE International Conference on Acoustics, Speech, and Signal Processing. Proceedings (Cat. No.01CH37221) (vol 6, pp 3461– 3464). Salt Lake City, UT, USA
22. Xiao T, Shi X, Zhou B, Wang X (2019) Comparative Study of EKF and UKF for SOC Estimation of Lithium-ion Batteries. In 2019 IEEE Innovative Smart Grid Technologies - Asia (ISGT Asia), Chengdu, China, pp 1570–1575
23. Luzi M, Paschero M, Rossini A, Rizzi A, Mascioli FMF (2016) Comparison between two nonlinear Kalman filters for reliable SoC estimation on a prototypal BMS. In IECON 2016–42nd Annual Conference of the IEEE Industrial Electronics Society. Italy, Florence, pp 5501–5506
24. Zhang T, Yang S, Hu J, Gao J, Liu D (2020) State of charge estimation of lithium battery based on FFRLS-SRUKF Algorithm. In 2020 IEEE 3rd International Conference on Electron- ics Technology (ICET), Chengdu, China, pp 433–437
25. Wang K, Feng X, Pang JB, Ren J, Duan CX, Li LW (2020) State of charge (SOC) estimation of lithium-ion battery based on adaptive square root unscented Kalman filter. Int J Electrochem Sci 15(9):9499–9516
26. Liu SL, Cui NX, Zhang CH (2017) An adaptive square root unscented Kalman filter approach for state of charge estimation of lithium-ion batteries. Energies 10(9):1–15
27. Ma L, Liu Z, Meng X (2010) Autonomous optical navigation based on adaptive SR-UKF for deep space probes. In Proceedings of the 29th Chinese Control Conference, Beijing, China, pp 321–325
28. Ouyang Q, Ma R, Wu ZX, Xu GT, Wang ZS (2020) Adaptive square-root unscented Kalman filter-based state-of-charge estimation for lithium-ion batteries with model parameter online identification. Energies 13(18):1–14
29. Asl RM, Hagh YS, Simani S, Handroos H (2019) Adaptive square-root unscented Kalman filter: an experimental study of hydraulic actuator state estimation. Mech Syst Signal Process 132:670–691
30. Zhou Y et al (2013) A new adaptive square-root unscented Kalman filter for nonlinear systems. Applied Mechanics and Materials, vol 300–301, Trans Tech Publications, Ltd., pp 623–626

31. Fusco D, Porpora F, Di Monaco M, Nardi V, Tomasso G (2022) High performance batery SoC estimation method based on an adaptive square-root unscented Kalman filter. In 2022 International Symposium on Power Electronics, Electrical Drives, Automation and Motion (SPEEDAM). Sorrento, Italy 424–429
32. Xiong R, Cao J, Yu Q, He H, Sun F (2017) Critical review on the batery state of charge estimation methods for electric vehicles. Ieee Access 6:1832–1843
33. Wang TP, Chen SZ, Ren HB, Zhao YZ (2018) Model-based unscented Kalman filter observer design for lithium-ion batery state of charge estimation. Int J Energy Res 42(4):1603–1614
34. Xi Z, Dahmardeh M, Xia B, Fu Y, Mi C (2019) Learning of batery model bias for effective state of charge estimation of lithium- ion bateries. IEEE Trans Veh Technol 68(9):8613–8628
35. Liu F, Liu T, Fu Y (2015) An improved SoC estimation algorithm based on artificial neural network. In 2015 8th International Symposium on Computational Intelligence and Design (ISCID). Hangzhou, China, pp 152–155
36. He HW, Xiong R, Fan JX (2011) Evaluation of lithium-ion batery equivalent circuit models for state of charge estimation by an experimental approach. Energies 4(4):582–598
37. Lai X, Zheng YJ, Sun T (2018) A comparative study of different equivalent circuit models for estimating state-of-charge of lithium-ion bateries. Electrochim Acta 259:566–577
38. Yuan HY, Han YJ, Zhou Y, Chen ZK, Du J, Pei HL (2022) State of charge dual estimation of a Li-ion batery based on variable forgetting factor recursive least square and multi-innovation unscented Kalman filter algorithm. Energies 15(4):1–22
39. Lao ZZ, Xia BZ, Wang W, Sun W, Lai YZ, Wang MW (2018) A novel method for lithium-ion batery online parameter identification based on variable forgetting factor recursive least squares. Energies 11(6):1–16
40. Li YW, Wang C, Gong JF (2016) A combination Kalman filter approach for state of charge estimation of lithium-ion batery considering model uncertainty. Energy 109:933–946
41. Sun XD, Ji JR, Ren BY, Xie CX, Yan D (2019) Adaptive forgetting factor recursive least square algorithm for online identification of equivalent circuit model parameters of a lithium-ion batery. Energies 12(12):1–15
42. Xu A (2021) novel adaptive dual extended Kalman filtering algorithm for the Li-ion batery state of charge and state of health co-estimation. Int J Energy Res 45(10):14592–14602